

MILD: Multi-Layer Diffusion Strategy for Complex and Precise Multi-IP Aware Human Erasing

Jinghan Yu^{1*}, Zhiyuan Ma^{1†}, Yue Ma², Kaiqi Liu³, Yuhang Wang¹, Jianjun Li⁴

¹THU, ²HKUST, ³NJU, ⁴HUST
jinghanyu0917@gmail.com, mzyth@tsinghua.edu.cn



Figure 1: The figure exhibits MILD (**our method**) can robustly handle three critical challenges in human erasing: *Human-Human Occlusion*, *Human-Object Entanglement*, and *Human-Background interferences* and can achieve clean and artifact-free removal results across diverse scenarios. Note each case shows the input and corresponding output pair.

Abstract

Recent years have witnessed the remarkable success of diffusion models, especially in various image-customized tasks. Previous works have achieved notable advances on simple human-oriented erasing task by leveraging explicit mask guidance and semantic-aware inpainting paradigm. Despite this progress, existing methods still struggle with significant human removal challenges raised by “*Multi-IP Interactions*” under more complex realistic scenarios such as *human-human occlusions*, *human-object entanglements* and

human-background interferences. These approaches are typically limited by: **1) Dataset deficiency**. They basically lack large-scale multi-IP datasets, especially those covering complex scenarios such as *dense occlusions*, *camouflaged or distracted backgrounds* and *diverse IP interactions*. **2) Lack of spatial decoupling**. Most methods lack effective spatial decoupling strategies to disentangle different foreground instances from the background, which limits their ability to achieve targeted human removal and clear background inpainting. These limitations result in performance degradation in precisely erasing overlapping individuals and restoring occluded regions in real-world scenes. In this work, we first introduce a high-quality human erasing dataset, **MILD dataset**, capturing diverse pose variations, occlusions, and complex

*Work done during internship.

†Corresponding author.

backgrounds in multi-IP interactive scenarios. Building on this foundation, we propose **Multi-Layer Diffusion (MILD)**, a novel multi-layer diffusion strategy for complex and precise multi-IP aware human erasing. Specifically, MILD first decomposes the traditional generation process into semantically separated denoising pathways, enabling independent reconstruction of each foreground instance and the background. To enhance human-centric understanding, we introduce Human Morphology Guidance, a plug-and-play guidance module that integrates pose, parsing, and spatial relations into the generation process, improving the morphological awareness and promoting more effective restoration. We further present Spatially-Modulated Attention, an adaptive mechanism that leverages spatial mask priors to effectively modulate attention across semantic regions, resulting in fewer boundary artifacts and mitigated semantic leakage. Extensive experiments demonstrate that MILD consistently outperforms state-of-the-art methods on challenging human erasing benchmarks. Our project page is available at: <https://mild-multi-layer-diffusion.github.io/>.

1 Introduction

Object removal aims to eliminate user-specified regions and synthesize visually coherent, context-consistent backgrounds Jampani et al. [2021], Xu et al. [2023]. This capability supports a wide range of applications, including photo editing, privacy preservation, and interactive content creation Yu et al. [2018], Liu et al. [2018]. However, achieving both thorough removal and faithful background restoration remains a challenging task, especially in scenarios involving multiple interacting instances and dense occlusions.

Early non-parametric methods Criminisi et al. [2004], Barnes et al. [2009] repainted erased regions by copying patches from visible areas, but often produce repetitive textures and fail in complex scenes. Afterwards, GAN-based models Pathak et al. [2016], Iizuka et al. [2017], Yu et al. [2018], Nazeri et al. [2019] introduce adversarial learning to enhance visual realism, yet suffer from global inconsistency and instability under large masks. Recently, diffusion-based models Song et al. [2021], Avrahami et al. [2023], Yang et al. [2023a] have achieved competitive performance by leveraging large-scale pretrained generative priors Rombach et al. [2022b], Ekin et al. [2024]. These models Zhuang et al. [2024], Yildirim et al. [2023] excel in generating diverse content, but remain limited in eliminating objects in complex multi-instance scenarios. For example, in Figure 4, standard LDM always fails to remove the target cleanly and instead hallucinates a new human-like figure at the masked region. Notably, the generated content retains dominant visual hints, such as “human”, implying that semantic features from the removed subject have leaked into the generation process.

These limitations highlight a fundamental challenge: *most existing methods treat object removal as an unified generation task, without explicitly decoupling the generation pathways for different foreground instances*. This framework often leads to semantic interference and content entanglement, especially in multi-IP or object-dense scenes, where features from one instance may bleed into others and degrade both the quality and controllability of the output.

To address these challenges, we introduce **Multi-Layer Diffusion (MILD)**, a diffusion-based strategy that reformulates human erasing as a disentangled, layer-wise, instance-aware generation process. As illustrated in Figure 1, MILD achieves high-fidelity removal in three representative challenges: human-human occlusions, human-object entanglements, and human-background interferences, which represent typical scenarios where existing methods tend to perform suboptimally. Our contributions are threefold:

- **MILD dataset.** A high-quality human erasing dataset is curated capturing diverse scenes with challenging poses, occlusions, and human-instance interactions. This dataset provides paired images with precise removal masks and realistic background, enabling rigorous evaluation of human erasing models in real-world scenarios.
- **Multi-Layer Diffusion Strategy (MILD).** We propose a MILD backbone that decomposes generation process into multiple semantically separated LoRA-based generation pathways, producing composable outputs corresponding to masked instances and the background. To further enhance performance, we introduce Human Morphology Guidance for instance-level understanding and Spatially-Modulated Attention for spatially conditioned attention control, enabling precise removal with minimal semantic leakage in complex scenes.
- **Comprehensive Experiments.** Extensive experiments on both real-world and synthetic datasets evaluate the effectiveness of our MILD strategy using diverse quantitative metrics and human evaluations. The ablation studies further demonstrate the individual contributions of Human Morphology Guidance and Spatially-Modulated Attention. Collectively, the results confirm that MILD achieves state-of-the-art performance in removal accuracy and background fidelity, outperforming existing human erasing baselines.

2 Related Work

Image Inpainting Image inpainting aims to restore missing or occluded regions in a visually coherent and semantically consistent manner in various scenarios Sargsyan et al. [2023], Zhou et al. [2020], Wang et al. [2024], Yoon and Cho [2024]. Traditional methods relied on patch propagation Hays and Efros [2007], Ding et al. [2019], transferring low-level textures from visible regions but failing in semantically complex scenes. With the rise of deep learning, the encoder-decoder Zhou et al. [2023], Cao et al. [2023], Altinel et al. [2018], Li et al. [2020a], Yi et al. [2020a] and GAN-based architectures Iizuka et al. [2017], Yu et al. [2018], Zeng et al. [2019] have significantly improved structural plausibility and perceptual quality, further enhanced by edge guidance Nazeri et al. [2019] and attention mechanisms Yu et al. [2018]. Diffusion-based methods Lugmayr et al. [2022], Saharia et al. [2022] have recently achieved strong generation performance by operating in latent spaces guided by powerful pretrained priors, but they often lack precise spatial control or instance-level disentanglement. Methods like SDXL Inpainting Podell et al.

Given an input image and N target masks $\{M_k\}_{k=1}^N$, MILD Backbone produces N foreground layers and a clean background layer. Each foreground branch is conditioned on its corresponding mask and reconstructs the associated subject, while the background branch synthesizes the unobstructed environment with all instances removed. To avoid redundant parameters and enable scalability, we adopt a shared UNet backbone with LoRA adapters. A single set of low-rank parameters is used across all foreground branches, while the background branch maintains an independent set. Formally, each LoRA modification is defined as:

$$\Delta W_p^{(b)} = \alpha_p^{(b)} B_p^{(b)} A_p^{(b)}, \quad p \in \{Q, K, V\}, b \in \{\text{fg}, \text{bg}\}, \quad (1)$$

where $A_p^{(b)} \in \mathbb{R}^{r \times d}$, $B_p^{(b)} \in \mathbb{R}^{d \times r}$, and $\alpha_p^{(b)}$ is a learnable scaling factor that supports concurrent training and inference of all branches, and facilitates interaction between instance-level predictions and global background restoration.

During training, each foreground branch learns to reconstruct its assigned region by utilizing the loss:

$$\mathcal{L}_k = \|M_k \odot (\epsilon - \epsilon_k)\|_2^2, \quad (2)$$

where $\epsilon \sim \mathcal{N}(0, 1)$ is standard Gaussian noise and ϵ_k denotes the prediction from the k -th branch. The background branch predicts noise over the entire image using the loss:

$$\mathcal{L}_{\text{bg}} = \|\epsilon - \epsilon_{\text{bg}}\|_2^2. \quad (3)$$

The total loss is formulated by combining the foreground and background losses as follows:

$$\mathcal{L}_{\text{total}} = \lambda_t \sum_{k=1}^N \mathcal{L}_k + \mathcal{L}_{\text{bg}}, \quad (4)$$

$$\lambda_t = \begin{cases} 0, & t < t_0 \\ \lambda \cdot \frac{t-t_0}{t_1-t_0}, & t_0 \leq t \leq t_1, \\ \lambda, & t > t_1 \end{cases}$$

where λ_t gradually increases to stabilize training. We adopt a staged strategy, first optimizing the background branch before introducing foreground supervision through ramp-up.

During inference, MILD produces composable outputs:

$$\{\text{Layer}_1, \dots, \text{Layer}_N, \text{Background}\}, \quad (5)$$

where each Layer_k represents an individual instance x_k . These layers can be selectively combined to reconstruct arbitrary subsets by removing the instance in $\mathcal{R} \subseteq \{1, 2, \dots, N\}$ as:

$$x_{\text{final}} = \left(\sum_{k \notin \mathcal{R}} M_k \odot x_k \right) + \left(\left(1 - \sum_{k \notin \mathcal{R}} M_k \right) \odot x_{\text{bg}} \right), \quad (6)$$

where \mathcal{R} denotes the set of instances to remove. For each $k \in \mathcal{R}$, the corresponding layer is excluded from the composite and automatically filled by the background layer x_{bg} . This layered formulation supports controllable recombination and improves reconstruction fidelity through joint foreground-background supervision.

Algorithm 1: MILD Training

Require: Image input: x , masks $\{M_k\}_{k=1}^N$
Require: Condition inputs: text prompt c_{text} , pose key-points P , parsing maps S

- 1: **// Human Morphology Guidance**
- 2: $F_{\text{pose}}, F_{\text{parse}} \leftarrow \text{PoseEncoder}(P, S)$
- 3: $Z_{\text{pose}}, Z_{\text{parse}} \leftarrow \text{LinearProj}(F_{\text{pose}}, F_{\text{parse}})$
- 4: **for** $k = 1$ to N **do**
- 5: $M_{\text{others}}^{(k)} \leftarrow \text{Aggregate}(\{M_j\}_{j \neq k})$
- 6: $Z_{\text{mask}}^{(k)} \leftarrow \text{MaskEncoder}(M_{\text{others}}^{(k)})$
- 7: $C^{(k)} \leftarrow \text{Concat}(Z_{\text{text}}, Z_{\text{pose}}, Z_{\text{parse}}, Z_{\text{mask}}^{(k)})$
- 8: **end for**
- 9: $C_{\text{bg}} \leftarrow \text{Concat}(c_{\text{text}}, T_{\text{pose}}, T_{\text{parse}})$
- 10: **// Dual LoRA Training**
- 11: **for** each timestep t and noise ϵ **do**
- 12: $z_t \leftarrow \sqrt{\alpha_t} z + \sqrt{1 - \alpha_t} \epsilon$
- 13: **for** $k = 1$ to N **do**
- 14: $\mathcal{L}_k \leftarrow \|(1 - M_k) \odot (\epsilon - \epsilon_k)\|_2^2$ {Foreground branch}
- 15: **end for**
- 16: $\mathcal{L}_{\text{bg}} \leftarrow \|\epsilon - \epsilon_{\text{bg}}\|_2^2$ {Background branch}
- 17: $\mathcal{L}_{\text{total}} \leftarrow \lambda_t \sum_{k=1}^N \mathcal{L}_k + \mathcal{L}_{\text{bg}}$
- 18: **end for**

3.2 Human Morphology Guidance

Although the dedicated Layered LoRA diffusion backbone lays the foundation for disentangling instance layers, fine-grained instance awareness remains essential for accurately removing targets and preserving body structures in spatially overlapping scenarios. To handle such complex scenarios, we introduce Human Morphology Guidance (HMG), a plug-and-play module that introduces fine-grained, human-centric priors into the denoising process.

As illustrated in Algorithm 1, HMG is seamlessly integrated into the MILD backbone by embedding pose and parsing information into the conditioning signals for both foreground and background branches. Specifically, preprocessed posture and parsing maps are separately encoded, flattened, linearly projected, and concatenated to form comprehensive human features, as shown in Figure 2 (b).

To further enhance spatial reasoning, we introduce a lightweight mask-based conditioning scheme that explicitly models neighboring instances. For each instance k , a context mask is constructed as:

$$M^{(k)} = \text{clamp}\left(\sum_{j \neq k} M_j, 0, 1\right), \quad (7)$$

which captures the spatial layout of surrounding instances, providing instance-aware guidance for precise IP localization. This mask is encoded through a shallow convolutional layer and concatenated with the target’s mask embedding and human features. Together, these spatially-aware priors provide stronger guidance for accurately separating instances, particularly in occluded scenarios.

By integrating explicit morphological and spatial cues, HMG significantly enhances instance-level disambiguation,

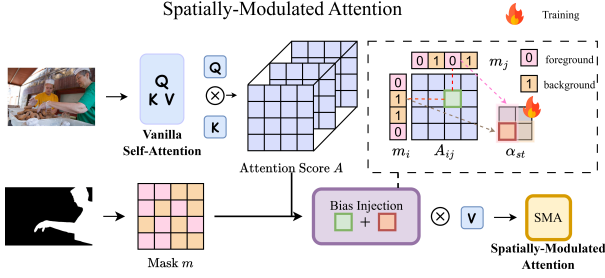


Figure 3: Illustration of the proposed *Spatially-Modulated Attention (SMA)* mechanism. For each query-key pair (i, j) , an spatial bias α_{st} is applied to the vanilla attention score A_{ij} , where $s = m_i$ and $t = m_j$ indicate their foreground/background status.

especially in challenging scenes involving occlusions, uncommon poses, or partially visible subjects.

3.3 Spatially-Modulated Attention

The original attention mechanisms utilize the entire context to generate reasonable background, but this leads to semantic leakage due to the unrestricted interactions between foreground and background tokens. To mitigate this, we propose Spatially-Modulated Attention (SMA), a lightweight module that enforces spatially constrained attention based on mask boundaries, as shown in Figure 3.

In standard self-attention, logits are computed as:

$$A_{ij} = \frac{Q_i K_j^T}{\sqrt{d_k}}. \quad (8)$$

To control attention flow across semantic separated regions, SMA introduces a learnable bias based on the binary masks m_i and m_j of tokens i and j :

$$\tilde{A}_{ij} = A_{ij} + \sum_{s,t \in \{0,1\}} \alpha_{st} \mathbb{1}[m_i = s, m_j = t], \quad (9)$$

where α_{st} are trainable parameters that modulate attention flow between foreground and background regions. The indicator function $\mathbb{1}[m_i = s, m_j = t]$ evaluates to 1 when token i belongs to region s and token j to region t , and 0 otherwise. For instance, α_{10} controls how effective a foreground token attends to the background.

Initialized with zero, these biases preserve the vanilla attention at the start and enabling adaptive spatial modulation during training. This enables explicit control over cross-region interactions without altering the attention mechanism itself. With this selective suppression, the attention flow learns to “attend to what it should” and mitigates leakage across masked boundaries. Integrated with MILD backbone and HMG, SMA improves the semantic isolation and artifacts removal in challenging multi-IP scenes.

4 Experiments

4.1 Experimental Setup

Datasets We conduct comprehensive evaluations on two datasets to assess both task-specific performance and cross-

domain generalization: 1) *Our MILD Dataset*: We construct a high-quality dataset specifically tailored for multi-IP erasure. The dataset comprises 10,000 image pairs featuring complex human interactions, diverse body poses, challenging occlusions, and a wide range of background contexts. The detailed information is introduced in Appendix A. 2) *OpenImages Dataset*: To evaluate generalization beyond human-centric scenarios, we randomly sample 1,000 images from OpenImages V5 Kuznetsova et al. [2020], covering diverse object categories and photographic conditions.

Implementation Details We train MILD LoRA on 20,000 images, including 10,000 real-world pairs from our curated MILD dataset and 10,000 synthetic samples generated by compositing segmented humans onto OpenImages backgrounds with random cropping and mask augmentation. The baseline model Podell et al. [2023] is optimized using AdamW Loshchilov and Hutter [2019] with a learning rate of $1e-6$, batch size 4, and trained for 20,000 iterations. Human Morphology Guidance leverages pose maps from OpenPose Cao et al. [2017] and parsing maps from SCHP Li et al. [2020b], preprocessed prior to training. A staged training scheme is adopted: the background branch is trained first, followed by a linear ramp-up of foreground losses after 8,000 steps. The model employs a UNet backbone within a latent diffusion framework, equipped with rank-16 LoRA modules (scaling factor 16). Inference uses 25 DDIM steps at 512×512 resolution. All experiments are conducted on NVIDIA A800 GPUs.

Baseline Comparisons We compare against a diverse set of state-of-the-art object removal methods, including SDXL Inpainting Podell et al. [2023], LaMa Suvorov et al. [2022], PowerPaint Zhuang et al. [2024], Inst-Inpaint Yildirim et al. [2023], CLIPAway Ekin et al. [2024], and RoRem Li et al. [2025], covering paradigms from mask-guided inpainting to instruction-based and vision-language-guided editing. To ensure a fair comparison, we adopt the official open-source implementations and reproduce results under a unified evaluation pipeline. All models are either used as publicly released or retrained with default settings on our datasets to ensure fair comparison.

Evaluation Metrics We adopt five complementary metrics to evaluate object removal quality from perceptual, semantic, and low-level fidelity perspectives. FID Heusel et al. [2017] evaluates global visual realism by comparing feature distributions of generated and real images, while LPIPS Zhang et al. [2018] focuses on local perceptual similarity based on deep features. DINO cosine similarity Caron et al. [2021] and CLIP Image Similarity Radford et al. [2021] measure semantic consistency by computing cosine similarity between the embeddings of generated and ground-truth images, capturing structural and high-level semantic alignment, respectively. Finally, PSNR Hore and Ziou [2010] quantifies pixel-level fidelity within the removed regions.

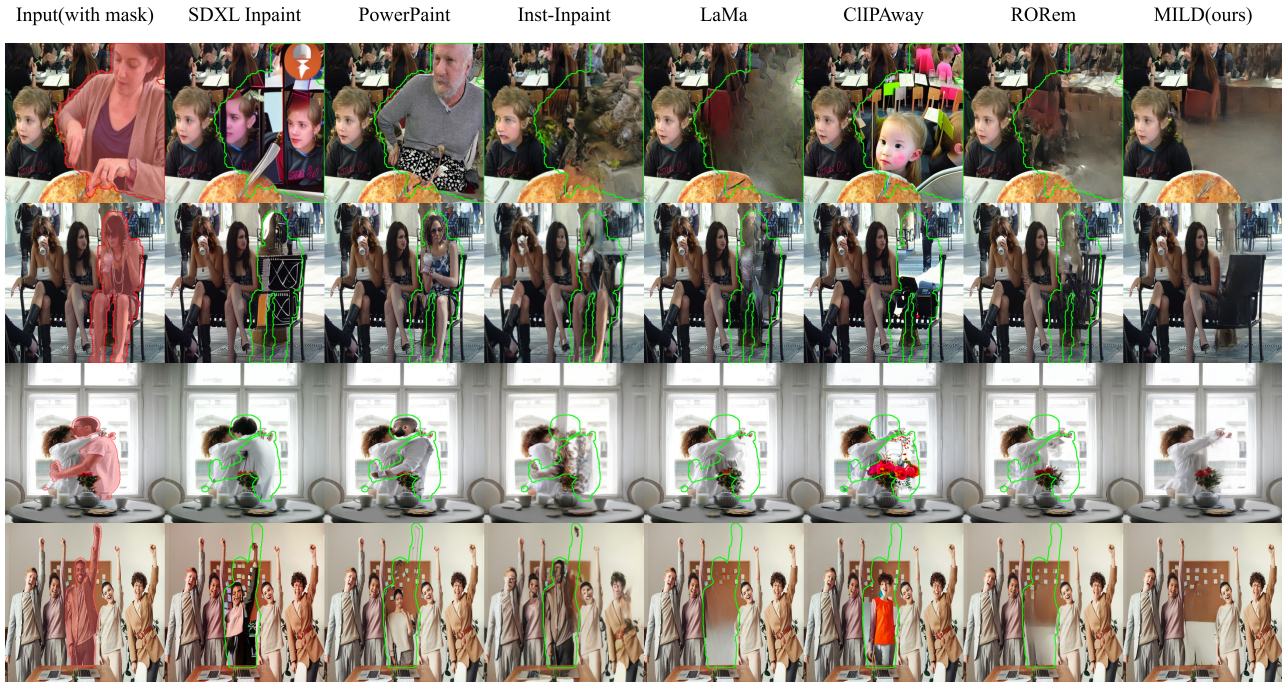


Figure 4: Qualitative results produced by MILD (ours) and other methods in real-world scenes. The masked regions (in red) and the corresponding removal results (in green) are highlighted for comparison.

4.2 Quantitative and Qualitative Comparisons

Table 1 summarizes the quantitative performance of various object removal methods on the MILD and OpenImages datasets. Our proposed MILD strategy consistently outperforms all baselines on the more challenging MILD dataset and remains highly competitive on OpenImages. Compared to the SDXL Inpainting baseline, MILD reduces FID and LPIPS by 54.53% and 61.57% respectively, reflecting significant improvement in visual realism and perceptual quality. It also achieves higher DINO, CLIP, and PSNR scores, demonstrating enhanced semantic consistency and pixel-level fidelity through its spatially-aware layered diffusion design. While LaMa performs well on FID and LPIPS in relatively simple scenes due to its smooth outputs, it underperforms in semantic metrics like DINO and CLIP, revealing limitations in understanding complex content. In contrast, MILD delivers superior results across all dimensions, particularly in complex human interactive scenes.

Figure 4 exhibits qualitative comparisons in challenging multi-IP scenarios. When the masked human occupies a large image region (**Row 1**), MILD generates semantically coherent and visually realistic content outperforming baselines. In scenes with complex human interactions (**Row 3**), it produces cleaner boundaries and fewer redrawings. Compared to existing methods, MILD effectively reduces hallucinations, avoids oversmoothing and blurring, and reconstructs sharper details in occluded regions. Notably, while LaMa performs well in simpler cases, it struggles with complex semantics and often introduces unrealistic blending (**Row 2**), which consistent with our quantitative results.

These results demonstrate the effectiveness of MILD’s layered diffusion strategy and spatially guided conditioning.

While traditional quantitative metrics provide valuable evaluations of model performance, they often fail to capture the direct naturalness and visual quality as perceived by human observers. To address this limitation, we conduct a comprehensive perceptual evaluation from both AI and human perspectives. The evaluation of both assessments are summarized in Figure 6, and the detailed experiment setting and the full table is shown in Appendix. Both AI and human evaluations consistently demonstrate that MILD achieves superior perceptual quality compared to baseline methods. Our method (MILD) achieves the highest success rate for both AI (82%) and human raters (78%), indicating consistent perceptual superiority. This comprehensive perceptual assessment validates the effectiveness of our approach in producing human-preferred removal results.

In summary, MILD achieves state-of-the-art performance on complex human interaction scenes, while also demonstrating competitive generalization to broader domains. It effectively balances visual realism, semantic alignment and perceptual quality across diverse human erasing scenarios.

4.3 Ablation Study

To evaluate the impact of the components in our multi-layer diffusion strategy, we conduct a step-by-step ablation study with both the quantitative and qualitative results in Table 2 and Figure 5. We progressively modify the baseline through four main experiments. We first incorporate the MILD Backbone into the SDXL inpainting baseline. Then the HMG and

Method	MILD Dataset					OpenImages Dataset				
	FID↓	LPIPS↓	DINO↑	CLIP↑	PSNR↑	FID↓	LPIPS↓	DINO↑	CLIP↑	PSNR↑
SDXL Inpaint	53.45	0.242	0.8398	0.8331	18.22	26.22	0.1346	0.8741	0.8751	21.88
PowerPaint	48.04	0.207	0.8901	0.8668	20.27	<u>10.56</u>	<u>0.0488</u>	<u>0.9649</u>	<u>0.9678</u>	31.04
Inst-Inpaint	—	—	—	—	—	11.42	0.4100	0.7400	0.8207	23.75
LaMa	<u>35.02</u>	0.164	<u>0.8909</u>	<u>0.8872</u>	<u>24.13</u>	10.38	0.0470	0.9192	0.9293	31.83
CLIPAway	48.86	0.230	0.8647	0.8605	19.49	22.73	0.1283	0.8973	0.8985	23.59
RoRem	40.41	0.196	0.8888	0.8810	22.35	18.23	0.0982	0.9095	0.9148	26.59
MILD (Ours)	24.20	0.093	0.9703	0.9499	26.24	17.86	0.0668	0.9829	0.9700	32.14

Table 1: Quantitative comparison of MILD and other methods on MILD and OpenImages datasets. Best results are **bold**, second best are underlined. Inst-Inpaint is excluded from the evaluation on MILD dataset as it lacks mask guidance, making it unsuitable for precise localization in multi-IP scenarios.



Figure 5: Qualitative ablation comparison of our method.

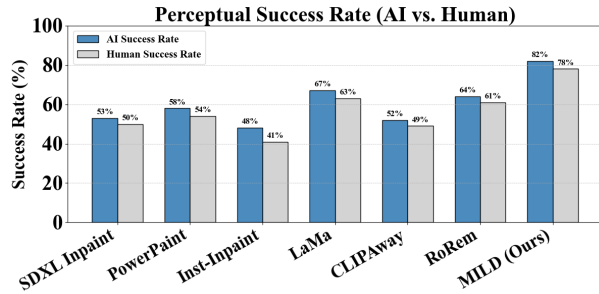


Figure 6: Comparison of AI and human success rates for object removal across different methods on the MILD dataset.

SMA modules are separately added into the structure. Finally, we evaluate the full MILD model, which integrates the MILD Backbone along with both HMG and SMA modules.

The SDXL Inpainting baseline performs poorly on the MILD dataset, often produces incomplete removals or hallucinated content when handling large or occluded subjects. Introducing MILD Backbone significantly improves both perceptual and semantic quality by disentangling generation into background and instance-specific foreground branches. This reduces the repainting phenomenon with 45.71% improvement in FID metric. Building on this backbone, HMG and SMA provide complementary enhancements. As shown in Figure 5, HMG helps to preserve body structure (row 2) and relieve the residual artifacts along object boundaries (row 1). Meanwhile, SMA focuses on refining the attention flow, effectively suppressing the unnatural mask bleeding and background leakage, resulting in smoother transitions and more coherent backgrounds. The full MILD model combines these advantages, achieving the best overall per-

Configuration	FID↓	LPIPS↓	DINO↑	CLIP↑	PSNR↑
SDXL Inpaint	53.45	0.242	0.8398	0.8331	18.22
+ MILD Backbone	29.02	0.142	0.9110	0.9025	23.45
+ HMG	26.10	0.120	0.9440	0.9312	24.67
+ SMA	25.10	0.105	0.9380	0.9227	25.21
MILD (Full)	24.20	0.093	0.9703	0.9499	26.24

Table 2: Ablation study on the MILD dataset.

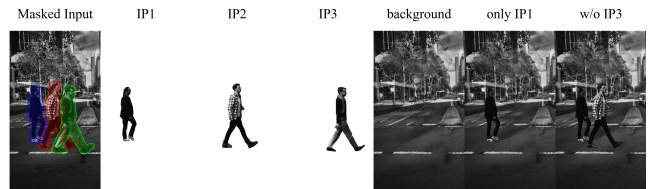


Figure 7: Illustration of MILD's compositional flexibility.

formance across all metrics. These results validate the non-redundant and effectiveness of our modular design.

4.4 Compositional Flexibility of Layered Outputs

Beyond achieving high-quality foreground removal and background restoration, MILD's layered diffusion design introduces a key advantage: the ability to flexibly recompose scenes using instance-specific foreground layers and a clean background. As shown in Figure 7, MILD generates disentangled outputs for each target, enabling selective combination to construct customized scenes. This allows users to separate specific individuals (e.g., only IP1), remove arbitrary targets (e.g., w/o IP3), or reconstruct any subset of the original scene. Such instance-aware recomposition offers fine-grained control over content manipulation, making MILD well-suited for interactive editing and scene simulation tasks. More details are shown in Appendix D.

5 Conclusion

We present *Multi-Instance Layered Diffusion*, a diffusion-based strategy reformulating inpainting as a layered, decoupled generation process for precise human erasing, supported by our curated, high-quality *MILD dataset*. MILD leverages HMG to provide instance-aware structure understanding, and employs SMA to bring spatially-conditioned

attention control, effectively reducing artifacts and improving reconstruction fidelity. Extensive experiments show that MILD outperforms existing inpainting baselines, achieving better semantic consistency, fewer artifacts, and more coherent scene reconstructions. MILD provides a promising direction for scaling precise diffusion-based inpainting to complex multi-object and open-domain removal tasks.

References

- Fazil Altinel, Mete Ozay, and Takayuki Okatani. Deep structured energy-based image inpainting. In *Proceedings of the International Conference on Pattern Recognition (ICPR)*, pages 423–428. IEEE Computer Society, 2018.
- Omri Avrahami, Dani Lischinski, and Ohad Fried. Blended latent diffusion. *ACM Transactions on Graphics*, 42(4): 1–11, 2023.
- Omer Bar-Tal, Dolev Ofri-Amar, Rafail Fridman, Yoni Kasten, and Tali Dekel. Text2live: Text-driven layered image and video editing. In *Proceedings of the European Conference on Computer Vision (ECCV)*, pages 707–723. Springer, 2022.
- Connelly Barnes, Eli Shechtman, Adam Finkelstein, and Dan B Goldman. Patchmatch: A randomized correspondence algorithm for structural image editing. *ACM Transactions on Graphics*, 28(3):1–11, 2009.
- Tim Brooks, Aleksander Holynski, and Alexei A Efros. Instructpix2pix: Learning to follow image editing instructions. In *Proceedings of the IEEE/CVF Conference on Computer Vision and Pattern Recognition*, pages 18392–18402, 2023.
- Chenjie Cao, Qiaole Dong, and Yanwei Fu. Zits++: Image inpainting by improving the incremental transformer on structural priors. *IEEE Transactions on Pattern Analysis and Machine Intelligence (TPAMI)*, 45(10):12667–12684, 2023.
- Zhe Cao, Tomas Simon, Shih-En Wei, and Yaser Sheikh. Realtime multi-person 2d pose estimation using part affinity fields. In *CVPR*, pages 7291–7299, 2017.
- Mathilde Caron, Hugo Touvron, Ishan Misra, Hervé Jégou, Julien Mairal, Piotr Bojanowski, and Armand Joulin. Emerging properties in self-supervised vision transformers. In *Proceedings of the IEEE/CVF International Conference on Computer Vision (ICCV)*, pages 9630–9640, 2021.
- Antonio Criminisi, Patrick Pérez, and Kentaro Toyama. Region filling and object removal by exemplar-based image inpainting. *IEEE Transactions on image processing*, 13(9):1200–1212, 2004.
- Ding Ding, Sundaresh Ram, and Jeffrey J. Rodríguez. Image inpainting using nonlocal texture matching and nonlinear filtering. *IEEE Transactions on Image Processing*, 28(4): 1705–1719, 2019.
- Yigit Ekin, Ahmet Burak Yildirim, Erdem Eren Caglar, Aykut Erdem, Erkut Erdem, and Aysegul Dundar. Clipaway: Harmonizing focused embeddings for removing objects via diffusion models. In *Advances in Neural Information Processing Systems*, volume 37, pages 17572–17601, 2024.
- Zigang Geng, Binxin Yang, Tiankai Hang, Chen Li, Shuyang Gu, Ting Zhang, Jianmin Bao, Zheng Zhang, Houqiang Li, Han Hu, Dong Chen, and Baining Guo. Instructdiffusion: A generalist modeling interface for vision tasks. In *Proceedings of the IEEE/CVF Conference on Computer Vision and Pattern Recognition (CVPR)*, pages 12709–12720. IEEE, 2024.
- Ligong Han, Song Wen, Qi Chen, Zhixing Zhang, Kunpeng Song, Mengwei Ren, Ruijiang Gao, Anastasis Sathopoulos, Xiaoxiao He, Yuxiao Chen, et al. Proxedit: Improving tuning-free real image editing with proximal guidance. In *Proceedings of the IEEE/CVF Winter Conference on Applications of Computer Vision (WACV)*, pages 4291–4301. IEEE, 2024.
- James Hays and Alexei A. Efros. Scene completion using millions of photographs. *ACM Transactions on Graphics (TOG)*, 26(3):4, 2007.
- Martin Heusel, Hubert Ramsauer, Thomas Unterthiner, Bernhard Nessler, and Sepp Hochreiter. Gans trained by a two time-scale update rule converge to a local nash equilibrium. In *Advances in neural information processing systems*, pages 6626–6637, 2017.
- Jonathan Ho, Ajay Jain, and Pieter Abbeel. Denoising diffusion probabilistic models. In *Advances in Neural Information Processing Systems*, volume 33, pages 6840–6851, 2020.
- Alain Hore and Djemel Ziou. Image quality metrics: Psnr vs. ssim. In *2010 20th International Conference on Pattern Recognition (ICPR)*, pages 2366–2369. IEEE, 2010.
- Edward J Hu, Yelong Shen, Phillip Wallis, Zeyuan Allen-Zhu, Yuanzhi Li, Shean Wang, Lu Wang, and Weizhu Chen. Lora: Low-rank adaptation of large language models. In *International Conference on Learning Representations (ICLR)*, 2022.
- Yuzhou Huang, Liangbin Xie, Xintao Wang, Ziyang Yuan, Xiaodong Cun, Yixiao Ge, Jiantao Zhou, Chao Dong, Rui Huang, Ruimao Zhang, and Ying Shan. Smartedit: Exploring complex instruction-based image editing with multimodal large language models. In *Proceedings of the IEEE/CVF Conference on Computer Vision and Pattern Recognition (CVPR)*, pages 8362–8371. IEEE, 2024.
- Satoshi Iizuka, Edgar Simo-Serra, and Hiroshi Ishikawa. Globally and locally consistent image completion. *ACM Transactions on Graphics*, 36(4):1–14, 2017.
- Jitesh Jain, Yuqian Zhou, Ning Yu, and Humphrey Shi. Keys to better image inpainting: Structure and texture go hand in hand. In *Proceedings of the IEEE/CVF Winter Conference on Applications of Computer Vision (WACV)*, pages 208–217. IEEE, 2023.
- Varun Jampani, Huiwen Chang, Kyle Sargent, Abhishek Kar, Richard Tucker, Michael Krainin, Dominik Kaeser, William T. Freeman, David Salesin, Brian Curless, and Ce Liu. Slide: Single image 3d photography with soft layering and depth-aware inpainting. In *Proceedings of the*

- IEEE/CVF International Conference on Computer Vision (ICCV)*, pages 12498–12507. IEEE, 2021.
- Yueru Jia, Yuhui Yuan, Aosong Cheng, Chuke Wang, Ji Li, Huizhu Jia, and Shanghang Zhang. Designedit: Multi-layered latent decomposition and fusion for unified & accurate image editing. *arXiv preprint arXiv:2403.14487*, 2024.
- Liyuan Jiang, Zhe Wang, Jianmin Bao, Wei Zhou, Dongdong Chen, Luowei Shi, and Houqiang Li. Smarteraser: Remove anything from images using masked-region guidance. In *Proceedings of the IEEE/CVF Conference on Computer Vision and Pattern Recognition (CVPR)*, pages 24452–24462, 2025.
- Diederik P Kingma and Max Welling. Auto-encoding variational bayes. In *Proceedings of the International Conference on Learning Representations (ICLR)*, 2014. URL <https://arxiv.org/abs/1312.6114>.
- Rolf Köhler, Christian J. Schuler, Bernhard Schölkopf, and Stefan Harmeling. Mask-specific inpainting with deep neural networks. In *Proceedings of the German Conference on Pattern Recognition (GCPR)*, pages 523–534. Springer, 2014.
- Alina Kuznetsova, Hassan Rom, Neil Alldrin, Jasper Uijlings, Ivan Krasin, Jordi Pont-Tuset, Shahab Kamali, Stefan Popov, Matteo Mallocci, Alexander Kolesnikov, et al. The open images dataset v4. *International Journal of Computer Vision*, 128(7):1956–1981, 2020.
- Jingyuan Li, Ning Wang, Lefei Zhang, Bo Du, and Dacheng Tao. Recurrent feature reasoning for image inpainting. In *Proceedings of the IEEE/CVF Conference on Computer Vision and Pattern Recognition (CVPR)*, pages 7757–7765. IEEE / Computer Vision Foundation, 2020a.
- Ke Li, Yiping Zhang, Lei Song, Xiaojuan Qi, Guanbin Huang, Liang Zhang, and Yu Qiao. Self-correction for human parsing. In *CVPR*, pages 8050–8059, 2020b.
- Rui Li, Tao Yang, Shilin Guo, and Lei Zhang. Rorem: Training a robust object remover with human-in-the-loop. In *Proceedings of the IEEE/CVF Conference on Computer Vision and Pattern Recognition (CVPR)*, pages 14024–14035, 2025.
- Ruibin Li, Ruihuang Li, Song Guo, and Lei Zhang. Source prompt disentangled inversion for boosting image editability with diffusion models. In *European Conference on Computer Vision (ECCV)*, 2024a.
- Shanglin Li, Bohan Zeng, Yutang Feng, Sicheng Gao, Xiuhui Liu, Jiaming Liu, Lin Li, Xu Tang, Yao Hu, Jianzhuang Liu, and Baochang Zhang. Zone: Zero-shot instruction-guided local editing. In *Proceedings of the IEEE/CVF Conference on Computer Vision and Pattern Recognition (CVPR)*, pages 6254–6263. IEEE, 2024b.
- Wenbo Li, Zhe Lin, Kun Zhou, Lu Qi, Yi Wang, and Jiaya Jia. Mat: Mask-aware transformer for large hole image inpainting. In *Proceedings of the IEEE/CVF Conference on Computer Vision and Pattern Recognition (CVPR)*, pages 10748–10758. IEEE, 2022.
- Yuheng Li, Haotian Liu, Qingyang Wu, Fangzhou Mu, Jianwei Yang, Jianfeng Gao, Chunyuan Li, and Yong Jae Lee. Gligen: Open-set grounded text-to-image generation. In *Proceedings of the IEEE/CVF Conference on Computer Vision and Pattern Recognition*, pages 22511–22521, 2024c.
- Guilin Liu, Fitsum A Reda, Kevin J Shih, Ting-Chun Wang, Andrew Tao, and Bryan Catanzaro. Image inpainting for irregular holes using partial convolutions. In *Proceedings of the European conference on computer vision*, pages 85–100, 2018.
- Ninghao Liu, Shengjia Li, Yilun Du, Antonio Torralba, and Josh B. Tenenbaum. Compositional visual generation with composable diffusion models. In *Proceedings of the European Conference on Computer Vision (ECCV)*, pages 423–439, Cham, 2022. Springer Nature Switzerland.
- Yiqing Liu, Haoyu Zhou, Bo Cui, Wenhao Shang, and Rongrong Lin. Erase diffusion: Empowering object removal through calibrating diffusion pathways. In *Proceedings of the IEEE/CVF Conference on Computer Vision and Pattern Recognition (CVPR)*, pages 2418–2427, 2025.
- Ilya Loshchilov and Frank Hutter. Decoupled weight decay regularization. In *International Conference on Learning Representations (ICLR)*, 2019.
- Erika Lu, Forrester Cole, Tali Dekel, Weidi Xie, Andrew Zisserman, David Salesin, William T Freeman, and Michael Rubinstein. Layered neural rendering for retiming people in video. *arXiv preprint arXiv:2009.07833*, 2020.
- Andreas Lugmayr, Martin Danelljan, Andrés Romero, Fisher Yu, Radu Timofte, and Luc Van Gool. Repaint: Inpainting using denoising diffusion probabilistic models. In *Proceedings of the IEEE/CVF Conference on Computer Vision and Pattern Recognition*, pages 11461–11471, 2022.
- Kamyar Nazeri, Eric Ng, Tony Joseph, Faisal Z Qureshi, and Mehran Ebrahimi. Edgeconnect: Structure guided image inpainting using edge prediction. In *Proceedings of the IEEE International Conference on Computer Vision Workshops*, 2019.
- Deepak Pathak, Philipp Krahenbuhl, Jeff Donahue, Trevor Darrell, and Alexei A Efros. Context encoders: Feature learning by inpainting. In *Proceedings of the IEEE conference on computer vision and pattern recognition*, pages 2536–2544, 2016.
- Dustin Podell, Zion English, Kyle Lacey, Andreas Blattmann, Tim Dockhorn, Jonas Müller, Joe Penna, and Robin Rombach. Sdxl: Improving latent diffusion models for high-resolution image synthesis. *arXiv preprint arXiv:2307.01952*, 2023.
- Alec Radford, Jong Wook Kim, Chris Hallacy, Aditya Ramesh, Gabriel Goh, Sandhini Agarwal, Girish Sastry, Amanda Askell, Pamela Mishkin, Jack Clark, et al. Learning transferable visual models from natural language supervision. In *International Conference on Machine Learning (ICML)*, pages 8748–8763, 2021.
- Robin Rombach, Andreas Blattmann, Dominik Lorenz, Patrick Esser, and Björn Ommer. High-resolution image synthesis with latent diffusion models. In *Proceedings*

- of the *IEEE/CVF Conference on Computer Vision and Pattern Recognition (CVPR)*, pages 10674–10685. IEEE, 2022a.
- Robin Rombach, Andreas Blattmann, Dominik Lorenz, Patrick Esser, and Björn Ommer. High-resolution image synthesis with latent diffusion models. In *Proceedings of the IEEE/CVF Conference on Computer Vision and Pattern Recognition (CVPR)*, pages 10674–10685. IEEE, 2022b.
- Olaf Ronneberger, Philipp Fischer, and Thomas Brox. U-net: Convolutional networks for biomedical image segmentation. In *International Conference on Medical Image Computing and Computer-Assisted Intervention (MICCAI)*, pages 234–241. Springer, 2015.
- Chitwan Saharia, William Chan, Huiwen Chang, Chris Lee, Jonathan Ho, Tim Salimans, David Fleet, and Mohammad Norouzi. Palette: Image-to-image diffusion models. In *ACM SIGGRAPH 2022 Conference Proceedings*, pages 1–10, 2022.
- Andranik Sargsyan, Shant Navasardyan, Xingqian Xu, and Humphrey Shi. Mi-gan: A simple baseline for image inpainting on mobile devices. In *Proceedings of the IEEE/CVF International Conference on Computer Vision (ICCV)*, pages 7301–7311. IEEE, 2023.
- Shelly Sheynin, Adam Polyak, Uriel Singer, Yuval Kirstain, Amit Zohar, Oron Ashual, Devi Parikh, and Yaniv Taigman. Emu edit: Precise image editing via recognition and generation tasks. In *Proceedings of the IEEE/CVF Conference on Computer Vision and Pattern Recognition (CVPR)*, pages 8871–8879. IEEE, 2024.
- Yang Song, Jascha Sohl-Dickstein, Diederik P. Kingma, Abhishek Kumar, Stefano Ermon, and Ben Poole. Score-based generative modeling through stochastic differential equations. In *International Conference on Learning Representations (ICLR)*. OpenReview.net, 2021.
- Wei Sun, Xuemeng Dong, Bo Cui, and Jie Tang. Attentive eraser: Unleashing diffusion model’s object removal potential via self-attention redirection guidance. In *Proceedings of the AAAI Conference on Artificial Intelligence*, volume 39, pages 20734–20742, April 2025.
- Roman Suvorov, Elizaveta Logacheva, Anton Mashikhin, Anastasia Remizova, Arsenii Ashukha, Aleksei Silvestrov, Naejin Kong, Harshith Goka, Kiwoong Park, and Victor Lempitsky. Resolution-robust large mask inpainting with fourier convolutions. In *Proceedings of the IEEE/CVF Winter Conference on Applications of Computer Vision*, pages 2149–2159, 2022.
- Yuxin Wang, Qianyi Wu, Guofeng Zhang, and Dan Xu. Learning 3d geometry and feature consistent gaussian splatting for object removal. In *Proceedings of the European Conference on Computer Vision (ECCV)*, pages 1–17. Springer, 2024.
- Daniel Winter, Matan Cohen, Shlomi Fruchter, Yael Pritch, Alex Rav-Acha, and Yedid Hoshen. Objectdrop: Bootstrapping counterfactuals for photorealistic object removal and insertion. In *Proceedings of the European Conference on Computer Vision (ECCV)*, pages 112–129. Springer, 2024.
- Shaoan Xie, Zhifei Zhang, Zhe Lin, Tobias Hinz, and Kun Zhang. Smartbrush: Text and shape guided object inpainting with diffusion model. In *Proceedings of the IEEE/CVF Conference on Computer Vision and Pattern Recognition (CVPR)*, pages 22428–22437. IEEE, 2023a.
- Shaoan Xie, Yang Zhao, Zhisheng Xiao, Kelvin C. K. Chan, Yandong Li, Yanwu Xu, Kun Zhang, and Tingbo Hou. Dreaminpainter: Text-guided subject-driven image inpainting with diffusion models. *CoRR*, abs/2312.03771, 2023b. URL <https://arxiv.org/abs/2312.03771>.
- Xingqian Xu, Shant Navasardyan, Vahram Tadevosyan, Andranik Sargsyan, Yadong Mu, and Humphrey Shi. Image completion with heterogeneously filtered spectral hints. In *Proceedings of the IEEE/CVF Winter Conference on Applications of Computer Vision (WACV)*, pages 4580–4590. IEEE, 2023.
- Gwanghyun Yang, Seonghyeon Song, Jong Chul Kim, and Wonmin Lee. Diffedit: Diffusion-based semantic image editing with mask guidance. In *Proceedings of the Eleventh International Conference on Learning Representations*, 2023a.
- Siyuan Yang, Lu Zhang, Liqian Ma, Yu Liu, Jingjing Fu, and You He. Magicremover: Tuning-free text-guided image inpainting with diffusion models. *CoRR*, abs/2310.02848, 2023b. URL <https://arxiv.org/abs/2310.02848>.
- Zili Yi, Qiang Tang, Shekoofeh Azizi, Daesik Jang, and Zhan Xu. Contextual residual aggregation for ultra high-resolution image inpainting. In *Proceedings of the IEEE/CVF Conference on Computer Vision and Pattern Recognition (CVPR)*, pages 7505–7514. IEEE, 2020a.
- Zili Yi, Qiang Tang, Shekoofeh Azizi, Daesik Jang, and Zhan Xu. Contextual residual aggregation for ultra high-resolution image inpainting. In *Proceedings of the IEEE/CVF Conference on Computer Vision and Pattern Recognition (CVPR)*, pages 7505–7514. IEEE, 2020b.
- Ahmet Burak Yildirim, Veysel Baday, Erkut Erdem, Aykut Erdem, and Ahmet Dundar. Inst-inpaint: Instructing to remove objects with diffusion models. *arXiv preprint arXiv:2304.03246*, 2023.
- Donggeun Yoon and Donghyeon Cho. Core-mpi: Consistency object removal with embedding multiplane image. In *Proceedings of the IEEE/CVF Conference on Computer Vision and Pattern Recognition (CVPR)*, pages 20081–20090. IEEE, 2024.
- Jiahui Yu, Zhe Lin, Jimei Yang, Xiaohui Shen, Xin Lu, and Thomas S Huang. Generative image inpainting with contextual attention. In *Proceedings of the IEEE conference on computer vision and pattern recognition*, pages 5505–5514, 2018.
- Yanhong Zeng, Jianlong Fu, Hongyang Chao, and Bain-ing Guo. Learning pyramid-context encoder network for high-quality image inpainting. In *Proceedings of the IEEE/CVF Conference on Computer Vision and Pattern Recognition*, pages 1486–1494, 2019.

- Richard Zhang, Phillip Isola, Alexei A Efros, Eli Shechtman, and Oliver Wang. The unreasonable effectiveness of deep features as a perceptual metric. In *Proceedings of the IEEE conference on computer vision and pattern recognition*, pages 586–595, 2018.
- Q. Zhangli, J. Jiang, D. Liu, L. Yu, X. Dai, A. Ramchandani, and P. Krishnan. Layout-agnostic scene text image synthesis with diffusion models. In *Proceedings of the IEEE/CVF Conference on Computer Vision and Pattern Recognition (CVPR)*, pages 7496–7506. IEEE Computer Society, 2024.
- Shengyu Zhao, Jonathan Cui, Yilun Sheng, Yue Dong, Xiao Liang, Eric I-Chao Chang, and Yan Xu. Large scale image completion via co-modulated generative adversarial networks. In *Proceedings of the International Conference on Learning Representations (ICLR)*, 2021.
- Gongjie Zheng, Xiangyu Zhou, Xihui Li, Zhenguo Qi, Ying Shan, and Xinxin Li. Layoutdiffusion: Controllable diffusion model for layout-to-image generation. In *Proceedings of the IEEE/CVF Conference on Computer Vision and Pattern Recognition (CVPR)*, pages 22490–22499. IEEE, 2023.
- Shangchen Zhou, Chongyi Li, Kelvin CK Chan, and Chen Change Loy. Propainter: Improving propagation and transformer for video inpainting. In *Proceedings of the IEEE International Conference on Computer Vision*, 2023.
- Tong Zhou, Changxing Ding, Shaowen Lin, Xinchao Wang, and Dacheng Tao. Learning oracle attention for high-fidelity face completion. In *Proceedings of the IEEE/CVF Conference on Computer Vision and Pattern Recognition (CVPR)*, pages 7677–7686. IEEE, 2020.
- Jiawei Zhuang, Yujun Zeng, Wei Liu, Chun Yuan, and Kaibin Chen. A task is worth one word: Learning with task prompts for high-quality versatile image inpainting. In *Proceedings of the European Conference on Computer Vision (ECCV)*, pages 195–211, Cham, September 2024. Springer Nature Switzerland.

Appendix

A Dataset and Code Availability

Dataset Construction. Our dataset comprises high-quality images collected from two primary sources: (1) a carefully curated subset of the OpenImages V5 dataset Kuznetsova et al. [2020], and (2) publicly available web images, gathered under fair use for academic research purposes. All images are manually verified to ensure diversity in scenes, human poses, occlusions, and background complexity.

Each image is annotated with pixel-level, instance-specific human masks. We further provide human-verified ground-truth completions to support supervised evaluation of object removal performance. Representative samples are shown in Figure 8. The complete dataset will be publicly released upon acceptance at: <https://mild-multi-layer-diffusion.github.io/dataset/>

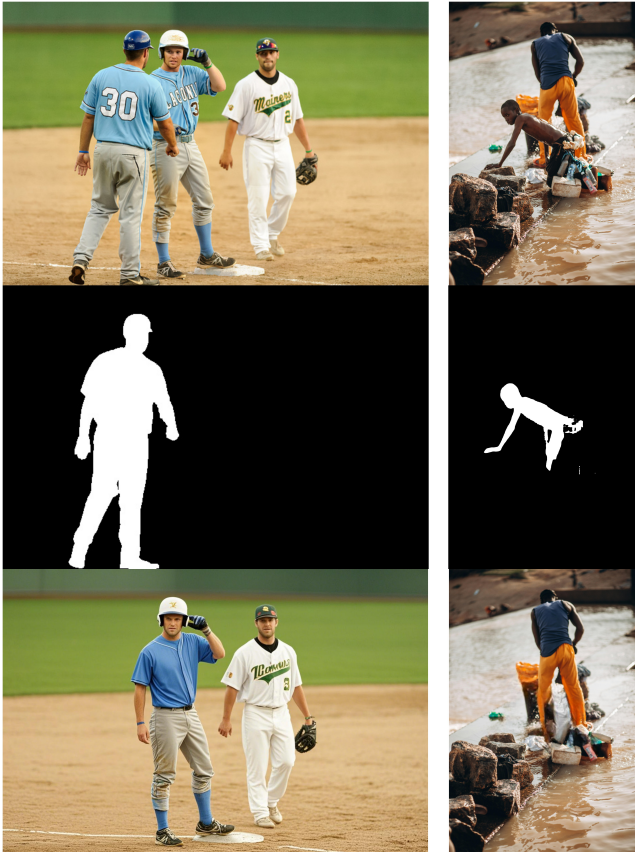


Figure 8: Sample data collected from MILD dataset.

Code and Model Release. To support future research and ensure reproducibility, we have created a public project page featuring representative examples and the paper abstract. The full codebase and pre-trained models will be made available upon acceptance at: <https://mild-multi-layer-diffusion.github.io/>

B More Related Works

Layered Generation and Controllability. Recent works on image generation have explored layered modeling and layout-based generation to enhance object awareness and controllability. Layered modeling works Jia et al. [2024], Lu et al. [2020] leverage multi-level structures through latent decomposition and scene-layer separation to enable semantically consistent editing. However, they often operate within a unified generation pathway and lack explicit instance disentanglement or spatial conditioning, making them less suitable for multi-object removal. Prompt- and layout-controllable generation works Liu et al. [2022], Zheng et al. [2023], Zhangli et al. [2024] aim to synthesize scenes from object-level prompts or layout priors. Although these methods offer flexible conditioning and structural guidance, they generally operate at a holistic level without explicit separation of foreground instances, limiting their capacity to handle occlusions or support fine-grained instance control. In contrast, our approach introduces a mask-aware, multi-branch generation framework that explicitly disentangles each foreground instance and the background into independent pathways. This layered formulation enables precise object removal, instance-level recomposition, and enhanced semantic fidelity through joint supervision.

C More Framework Details

To ensure reproducibility, we provide additional details of the training pipeline, architectural design, and spatial supervision strategies used in *LayeredUNet*. The model is optimized in stages (Algorithm 2), where a training controller gradually activates different generation branches. Each image is encoded into the latent space and perturbed with spatial offsets derived from the union of all masks. To stabilize learning, the background branch is initially protected by freezing its gradients, while foreground branches are progressively optimized with instance-specific conditioning.

Both foreground and background branches share a unified UNet backbone but use independent LoRA adapters. During the forward pass (Algorithm 3), we apply **Spatially-Modulated Attention (SMA)** in all attention layers across both branches, replacing standard self-attention. SMA enforces spatial constraints guided by the input masks, helping to prevent feature leakage and preserve structural consistency.

To further improve boundary quality and compositional integrity, optional modules such as layer exchange and boundary smoothing can be enabled. These help align overlapping regions and reduce visible seams. Additionally, the foreground branch is supervised using a **region-aware loss** that emphasizes both the core masked region and its boundaries via residual and gradient-based penalties, improving local coherence and mask adherence.

D More Experiments

D.1 More Quantitative Results

To further validate the robustness and generalizability of our method, we introduce the Structural Similarity Index Measure (SSIM) as an additional evaluation metric. Unlike

Algorithm 2: Training of LayeredUNet with Progressive Dual LoRA

Require: Input image x , mask set $\{M_k\}_{k=1}^N$, prompt c_{text} , optional pose P , parsing S

- 1: $z_0 \leftarrow \text{VAE}(x)$
- 2: $z_0 \leftarrow z_0 + \mathcal{E}_{\text{trans}}(\text{union}(\{M_k\}))$ {Inject spatial offsets}
- 3: $Z_{\text{pose}}, Z_{\text{parse}} \leftarrow \text{PoseEncoder}(P, S)$
- 4: $Z_{\text{text}} \leftarrow \text{TextEncoder}(c_{\text{text}})$
- 5: $Z_{\text{cond}} \leftarrow \text{Concat}(Z_{\text{text}}, Z_{\text{pose}}, Z_{\text{parse}})$
- 6: **for** each training step t **do**
- 7: stage $\leftarrow \text{GetTrainingStage}(t)$
- 8: $z_t \leftarrow \text{AddNoise}(z_0, t)$
- 9: **for** $k = 1$ to N **do**
- 10: $M_{\text{others}}^{(k)} \leftarrow \text{Aggregate}(\{M_j\}_{j \neq k})$
- 11: $Z_{\text{mask}}^{(k)} \leftarrow \text{MaskEncoder}(M_{\text{others}}^{(k)})$
- 12: $C_k \leftarrow \text{Concat}(Z_{\text{cond}}, Z_{\text{mask}}^{(k)})$
- 13: $\epsilon_k \leftarrow \text{UNet}(z_t, t, C_k, \text{branch} = \text{"fg"}, M_k)$
- 14: $\mathcal{L}_k \leftarrow \text{RegionLoss}(\epsilon_k, z_0, M_k)$
- 15: **end for**
- 16: $\epsilon_{\text{bg}} \leftarrow \text{UNet}(z_t, t, Z_{\text{cond}}, \text{branch} = \text{"bg"})$
- 17: $\mathcal{L}_{\text{bg}} \leftarrow \|\epsilon - \epsilon_{\text{bg}}\|_2^2$
- 18: $\mathcal{L}_{\text{total}} \leftarrow \lambda_t \sum_k \mathcal{L}_k + \mathcal{L}_{\text{bg}}$
- 19: **if** stage requires gradient protection **then**
- 20: FreezeLoRA("background")
- 21: **end if**
- 22: Backward($\mathcal{L}_{\text{total}}$), UpdateLoRA()
- 23: **end for**

FID, LPIPS, or CLIP-based perceptual scores, SSIM captures low-level structural consistency between the generated and ground-truth images, providing complementary insight into image fidelity.

As summarized in Table 3 (MILD dataset) and Table 4 (OpenImages dataset), our method consistently outperforms prior approaches across all major metrics, including the newly introduced SSIM. This further confirms that MILD not only produces perceptually realistic outputs but also preserves structural coherence with the surrounding context.

The inclusion of SSIM highlights MILD’s ability to maintain both global semantics and local structural details, reinforcing its effectiveness in complex object removal scenarios.

D.2 More Qualitative Results

To further demonstrate the effectiveness of our approach, we present additional qualitative comparisons against state-of-the-art baselines in diverse and challenging scenarios. These include scenes with multiple interacting persons, complex occlusions, cluttered backgrounds, and fine structural details such as limbs, shadows, and object boundaries.

As shown in Figure 9, our method produces more semantically consistent and visually coherent results compared to existing methods. In particular, our model excels at generating plausible textures, maintaining global scene structure, and avoiding common failure cases such as blurry artifacts, object duplication, or semantic distortions. These results fur-

Algorithm 3: Forward Pass of LayeredUNet with SMA

Require: Latent input z_t , timestep t , condition C , mask M , branch $\in \{\text{"foreground"}, \text{"background"}\}$

- 1: $z_t \leftarrow z_t + \mathcal{E}_{\text{trans}}(M)$ {Inject spatial offsets}
- 2: **for** each attention layer in UNet **do**
- 3: **if** branch = "foreground" **then**
- 4: $Q, K, V \leftarrow \text{LoRA}_{\text{fg}}(z_t, C)$
- 5: attn $\leftarrow \text{SMA}(Q, K, V)$
- 6: **else**
- 7: $Q, K, V \leftarrow \text{LoRA}_{\text{bg}}(z_t, C)$
- 8: attn $\leftarrow \text{SMA}(Q, K, V)$
- 9: **end if**
- 10: $z_t \leftarrow \text{Apply}(z_t, \text{attn})$
- 11: **if** layer exchange enabled **then**
- 12: $z_t \leftarrow z_t + \text{LayerExchange}(z_t)$
- 13: **end if**
- 14: $z_t \leftarrow z_t + \text{BoundarySmoothing}(z_t, M)$
- 15: **end for**
- 16: **return** $\epsilon_{\text{pred}} \leftarrow \text{UNetOutput}(z_t)$

ther validate the benefits of our layered generation strategy, human-centric guidance, and attention modulation.

All examples are selected from the test split of our curated dataset. Please refer to the project page for high-resolution images and interactive comparisons.

D.3 Inference Efficiency.

Table 5 summarizes the average inference time per image at 512×512 resolution using an A800 GPU with 25 diffusion steps. Despite incorporating a layered, multi-branch generation strategy, **MILD** maintains efficient runtime performance. Due to the shared UNet backbone and lightweight LoRA-based adaptation, our method achieves instance-aware generation without redundant computation overhead.

Compared to other diffusion-based baselines such as PowerPaint, CLIPAway, and RoRem, MILD demonstrates notably faster inference. While it supports text prompts to enhance generation precision, the impact on speed is minimal, resulting in comparable runtime to the SDXL Inpainting baseline. Although LaMa achieves the fastest runtime overall owing to its CNN-based architecture, it compromises significantly on visual fidelity and semantic accuracy, as evidenced by its performance in Table 4. Overall, MILD offers a favorable trade-off between generation quality and runtime efficiency.

D.4 AI evaluation.

Implementation details We evaluate perceptual quality using both AI-based and human-based protocols. For the AI evaluation, we employ GPT-4o to assess 100 randomly selected image pairs. Given a standardized prompt, GPT-4o performs a side-by-side visual inspection of the original and edited images and assigns four aspect-wise scores including *naturalness*, *semantic consistency*, *visual harmony*, and *artifact suppression*, each on a 1–10 scale. These are then averaged to produce an overall perceptual score. The model

Method	FID↓	LPIPS↓	DINO↑	CLIP↑	PSNR↑	SSIM↑
SDXL Inpaint	53.45	0.242	0.8398	0.8331	18.22	0.6984
PowerPaint	48.04	0.207	0.8901	0.8668	20.27	0.7569
LaMa	<u>35.02</u>	<u>0.164</u>	<u>0.8919</u>	<u>0.8872</u>	<u>24.13</u>	<u>0.7984</u>
CLIPAway	48.86	0.230	0.8647	0.8605	19.49	0.7046
RoRem	40.41	0.196	0.8888	0.8810	22.35	0.7521
MILD (Ours)	24.20	0.093	0.9703	0.9499	26.24	0.8341

Table 3: Quantitative comparison of MILD and other methods on MILD dataset. Best results are **bold**, second best are underlined.

Method	FID↓	LPIPS↓	DINO↑	CLIP↑	PSNR↑	SSIM↑
SDXL Inpaint	26.22	0.1346	0.8741	0.8751	21.88	0.8290
PowerPaint	<u>10.56</u>	<u>0.0488</u>	<u>0.9649</u>	<u>0.9678</u>	31.04	0.9638
Inst-Inpaint	11.42	0.4100	0.7400	0.8207	23.75	0.8023
LaMa	10.38	0.0470	0.9192	0.9293	31.83	0.9461
CLIPAway	22.73	0.1283	0.8973	0.8985	23.59	0.8276
RoRem	18.23	0.0982	0.9095	0.9148	26.59	0.8713
MILD (Ours)	17.86	0.0668	0.9829	0.9700	32.14	<u>0.9515</u>

Table 4: Quantitative comparison of object removal methods on the **OpenImages** dataset. Best results are **bold**, second best are underlined.

Table 5: Average inference time per image (in seconds), along with framework type and guidance type.

Method	Guidance Type	Time (s)
SDXL Inpaint	Text + Mask	1.79
PowerPaint	Text + Mask	6.21
Inst-Inpaint	Text-only	2.21
LaMa	Mask-only	1.50
CLIPAway	Text + Mask	4.76
RoRem	Text + Mask	4.15
MILD (Ours)	Text + Mask	1.91

also provides a binary decision indicating whether the object removal is **successful** or **unsuccessful**.

For the human evaluation, we recruit 20 participants to rate the same 100 image pairs. Each participant is asked to consider the above four aspects holistically and assign a single overall quality score between 1 and 10. Additionally, they indicate whether the result is **successful** or **unsuccessful**, based on the overall plausibility and absence of noticeable artifacts. Final human scores are computed by averaging all participant ratings, and success rate is calculated as the percentage of participants marking each result as successful.

AI & Human Evaluation Protocol To assess the perceptual quality of human erasing, we employ a unified evaluation protocol involving both AI-based and human-based assessments. In both cases, evaluators are presented with side-by-side comparisons of the original image (with the human present) and the edited result, and are asked to judge the visual plausibility of the removal without access to ground

truth.

For the AI evaluation, we use GPT-4o to score each image across four criteria, adapted from standard visual editing assessments: *naturalness*, *semantic consistency*, *visual harmony*, and *artifact suppression*. Each aspect is rated on a 1–10 scale, and the average of these scores is reported as the overall perceptual score. Additionally, GPT-4o provides a binary decision indicating whether the removal is considered **successful** or **unsuccessful**, based on visual realism and contextual coherence.

- **Naturalness:** Whether the filled region appears visually plausible and free from obvious artifacts.
- **Semantic Consistency:** Whether the inpainted content aligns semantically with the surrounding scene.
- **Visual Harmony:** Whether lighting, textures, and shadows in the edited region are consistent with the rest of the image.
- **Artifact Suppression:** Whether the result avoids seams, blurs, distortions, or other visual artifacts.

In the human evaluation, we recruit 20 participants to assess the same set of 100 images. Unlike the AI annotator, human raters do not score each aspect individually. Instead, they are instructed to consider all four criteria jointly and provide a single overall quality score (1–10) for each image, reflecting their holistic impression. They also indicate whether the removal is **successful** or **unsuccessful** according to the same definition used in the AI evaluation—namely, that a successful result should appear seamless, contextually appropriate, and free of noticeable flaws.

Final results are reported in terms of AI and human perceptual scores, along with success rates computed as the percentage of cases marked as successful.

Method	AI Overall	Human Overall	Success Rate
SDXL Inpaint	3.7	4.2	53% / 50%
PowerPaint	5.0	5.2	58% / 54%
Inst-Inpaint	4.7	4.8	48% / 41%
LaMa	6.4	6.3	67% / 63%
CLIPAway	3.9	4.0	52% / 49%
RoRem	5.4	5.4	64% / 61%
MILD (Ours)	8.3	8.4	82% / 78%

Table 6: Perceptual evaluation summary on the MILD dataset. AI and human scores reflect overall perceptual quality (1–10 scale).

Evaluation Results Table 6 summarizes the perceptual evaluation results from both AI and human annotators. Our method, **MILD**, consistently achieves the highest overall perceptual score among all compared approaches. It also attains the highest success rates from GPT-4o and from human raters, indicating strong agreement across evaluation modalities. Overall, these results confirm the effectiveness of our MILD strategy in producing perceptually convincing and contextually coherent removal outputs, outperforming prior methods in both automated and human assessments.

D.5 More Compositional Flexibility

Figure 10 provides a detailed visualization of MILD’s compositional flexibility. Given a masked input image containing three interacting persons (IP1–IP3), our model generates four disentangled outputs: one foreground layer per instance and a clean background. By selectively combining these layers, MILD enables the construction of diverse scene variants. As illustrated, we showcase six recomposed outputs, including single-subject isolation (e.g., only IP1), targeted removal (e.g., w/o IP2), and partial restoration (e.g., IP1 and IP3). This layered formulation supports fine-grained, user-controllable editing, and highlights the advantages of explicit instance-level generation over unified inpainting approaches.

E Limitations

Despite the strong performance of MILD in a wide range of challenging scenarios, several limitations remain. First, when the occluded region is particularly large, occupying up to two-thirds of the image, MILD may struggle to produce fully realistic completions. While the results are generally more perceptually plausible than those generated by existing baselines (see Figure 11, Row 1), the reconstruction of fine-grained background details is often imperfect due to limited contextual information. Second, in some instances, the generation produced by MILD tends to be overly conservative. Although the object is successfully removed and the result appears semantically coherent, the model may fail to fully restore the background content or reflect the underlying scene logic (see Figure 11, Row 2).

We consider these issues valuable directions for future research, particularly in enhancing hallucination capabilities under severe occlusion and developing more flexible gener-

ation mechanisms that better balance fidelity and expressiveness.

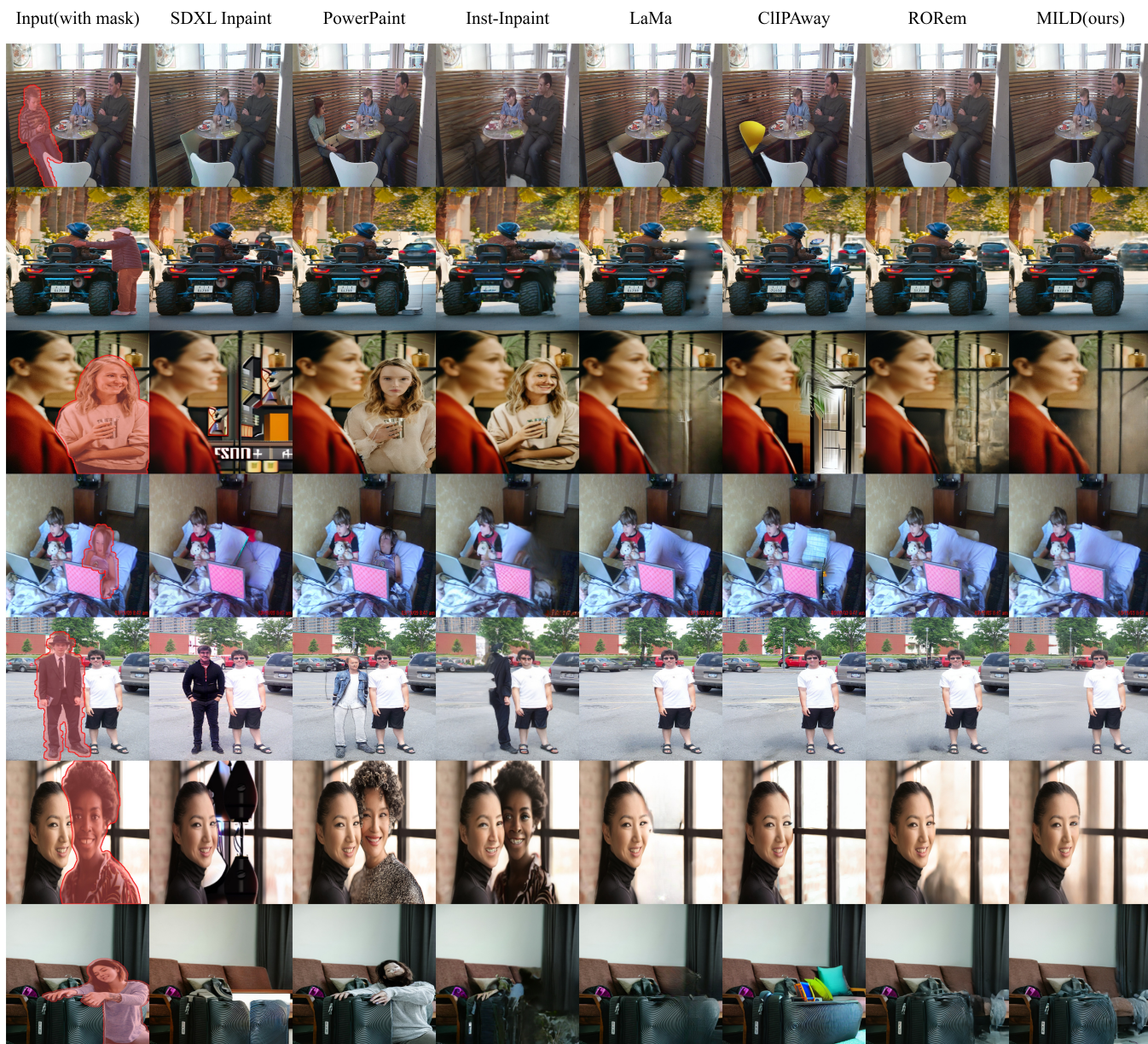


Figure 9: More Qualitative Comparisons between MILD and other methods on MILD dataset.

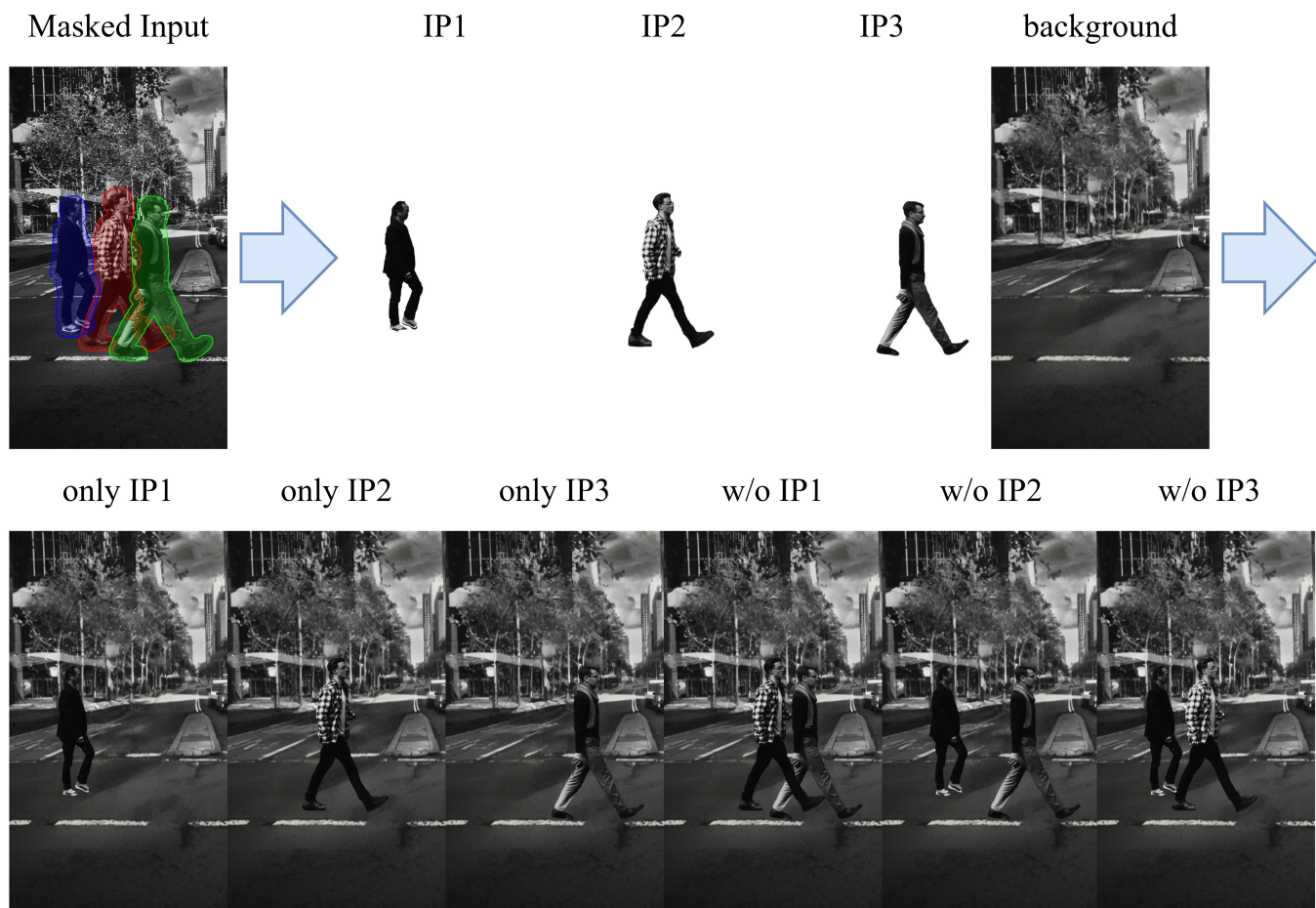


Figure 10: Compositional scene recomposition with MILD. Given a masked input with three foreground targets (IP1–IP3), we show the disentangled outputs and six representative recombinations enabled by our layered generation design.

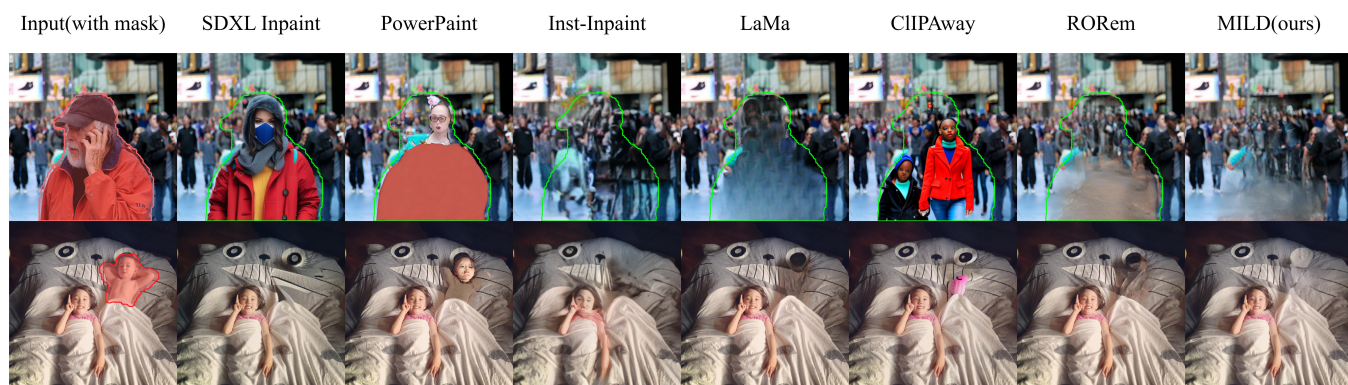


Figure 11: Failure example of MILD, along with other methods.